Geoscience Frontiers 11 (2020) 473–486

HOSTED BY

Contents lists available at ScienceDirect

Geoscience Frontiers

journal homepage: www.elsevier.com/locate/gsf

Research Paper

Modeling for critical state line of granular soil with evolution of grain size distribution due to particle breakage

Ching S. Chang *, Yibing Deng

Department of Civil and Environmental Engineering, University of Massachusetts, Amherst, MA, 01003, USA

ARTICLE INFO

Keywords:
Critical state void ratio
Particle breakage
Grain size distribution
Particle packing model
Granular material

ABSTRACT

Determination of the critical state line (CSL) is important to characterize engineering properties of granular soils. Grain size distribution (GSD) has a significant influence on the location of CSL. The influence of particle breakage on the CSL is mainly attributed to the change in GSD due to particle breakage. However, GSD has not been properly considered in modeling the CSL with influence of particle breakage. This study aims to propose a quantitative model to determine the CSL considering the effect of GSD. We hypothesize that the change of critical state void ratio with respect to GSD is caused by the same mechanism that influences of the change of minimum void ratio with respect to GSD. Consequently, the particle packing model for minimum void ratio proposed by Chang et al. (2017) is extended to predict critical state void ratio. The developed model is validated by experimental results of CSLs for several types of granular materials. Then the evolution of GSD due to particle breakage is incorporated into the model. The model is further evaluated using the experimental results on rockfill material, which illustrates the applicability of the model in predicting CSL for granular material with particle breakage.

1. Introduction

Critical state is defined as the state at which the soil continues to deform in shear at constant stress and constant void ratio (Roscoe et al., 1958). At this state, a unique relationship between the critical state void ratio (e_{cs}) and the mean effective stress (p') can be expressed by a critical state line (CSL) in the $e-\log p$' plane, which is independent of stress path including intermediate stress (Roscoe et al., 1958; Schofield and Wroth, 1968; Been et al., 1991; Riemer and Seed, 1997; Zhou et al., 2017). The CSL is a fundamental property, which has been widely used to characterize strength, deformation, and liquefaction behavior of granular soil (Schofield and Wroth, 1968; Been and Jefferies, 1985; Imam et al., 2005; Jefferies and Been, 2006).

Many investigators found that the location of a CSL in the $e-\log p$' plane is significantly influenced by particle breakage when granular soils undergo high stress. This observation has been found in experiments (Hardin, 1985; Biarez and Hicher, 1994; Verdugo and Ishihara, 1996; Hyodo et al., 2001; Carraro et al., 2009; Bandini and Coop, 2011; Yu, 2017) and in discrete element simulations (Muir Wood and Maeda, 2008; Sadrekarimi and Olson, 2011; Zhou et al., 2017; Ciantia et al., 2019).

Traditionally, a three-segment linear CSL in the $e-\log p$' plane (as the solid line shown in Fig. 1) has been adopted for the full range of p' (Been et al., 1991; Konrad, 1998; Russell and Khalili, 2004).

At the first segment, the stress level is very low where breakage is negligible, thus the grain size distribution (GSD) of the specimen keeps constant. At the second segment, the stress level is elevated where breakage becomes pronounced. Due to particle breakage, the CSL becomes steeper and the GSD at critical state changes with mean effective stress. At the third segment, the stress level is very high, but there is no further breakage because an ultimate GSD has been reached. Thus, the CSL becomes flatter.

The influence of particle breakage on CSL is mainly attributed to the evolution of GSD. Based on this viewpoint, Daouadji et al. (2001) first suggested that, instead of three-segment line, the CSL is related to a family of parallel lines (as the dashed lines shown in Fig. 1) where each line corresponds to a constant GSD. The second segment of the solid CSL was interpreted as a locus of end points of this family of dashed CSLs. Each point on the locus is at successively higher stresses and has more breakages. The changing GSD caused by the breakage leads to a steeper curve of the CSL. This family of parallel lines provide an alternative picture to the three-segment line. The dashed CSL moves downward with increasing particle breakage or increasing coefficient of uniformity of

* Corresponding author.
E-mail addresses: cchang@engin.umass.edu (C.S. Chang), yibingdeng@engin.umass.edu (Y. Deng).
Peer-review under responsibility of China University of Geosciences (Beijing).

https://doi.org/10.1016/j.gsf.2019.06.008
Received 30 May 2018; Received in revised form 25 April 2019; Accepted 29 June 2019
Available online 6 August 2019

gradation. This observation has also been found in experiments (Hu et al., 2011; Li et al., 2015; Xiao et al., 2016; Yu and Su, 2016). The role of GSD on the location of dashed CSL has been raised as a key question in mechanics of sands (Bandini and Coop, 2011).

Muir Wood and Maeda (2008) developed this idea further by suggesting a "grading state index", a parameter between 0 and 1 which was used to characterize the changed GSD due to particle breakage. The set of parallel dashed CSLs in Fig. 1 correspond to different grading state indices I_g. As breakage occurs, the grading state index increases, and the dashed CSL moves downward. The relationship between the dashed CSL and grading state index was used to account for the effect of breakage.

Other than the grading state index, various types of breakage indices were used to characterize the evolution of GSD due to particle breakage (Marsal, 1963; Hardin, 1985; Lade et al., 1996; Einav, 2007; Xiao and Liu, 2017). Attempts were also made to link the relationship between the dashed CSL with breakage index (Einav, 2007; Tengattini et al., 2016; Xiao and Liu, 2017).

However, this type of empirical relationship is obtained from fitting the experimental results, which is only applicable to the specific soil and the conditions used in the experiments. Furthermore, because this type of empirical relationship only uses grading/breakage index, which does not directly account for the influence of GSD. In this paper, we aim to develop an analytical model to predict the CSL with influence of particle breakage by directly considering GSD.

Herein, the particle packing model for minimum void ratio proposed by Chang et al. (2017) is extended to predict the CSL for granular soil considering the effect of GSD. In the following, in order to make the model extension more logical, we begin with the correlation analysis between minimum and critical state void ratios. Then the particle packing model is extended to predict the CSL considering the effect of GSD. Two cases are considered: for material without particle breakage and for material with particle breakage. For the case without particle breakage, the proposed model is verified by experimental results for four types of granular materials at small stress range. For the case with particle breakage, the proposed model is verified by a rockfill material with considerable particle breakage.

2. Rationale using particle packing model for e_{cs}

The minimum void ratio (e_{min}), achieved through the method specified by American Society for Testing and Materials (ASTM), is found to be highly influenced by GSD of the granular soil (Youd, 1973; Lade et al., 1998; Thevanayagam et al., 2002; Yilmaz, 2009). An analytical particle packing model has been developed and verified by comparing the measured and predicted minimum void ratios for sand-silt mixtures with various fines content (Chang et al., 2015) and for multi-sized granular soils with various GSD (Chang et al., 2017).

It is interesting to note that the model for minimum void ratio was extended to predict the maximum void ratio (e_{max}) with great accuracy (Chang et al., 2016). The good performance was expected because a very strong correlation was noted between e_{max} and e_{min} (Cubrinovski and Ishihara, 2002; Chang et al., 2016). Thus, it was hypothesized that the change of maximum void ratio with respect to GSD is caused by the same particle mixing mechanism that influences the change of minimum void ratio with respect to GSD.

Along this line of reasoning, we exam the correlation between the critical state void ratio e_{cs} and the minimum void ratio e_{min}. Fig. 2a shows a strong correlation between e_{cs} and e_{min} for quartz silty-sand at three different stress levels (i.e., p' = 33–45, 185–250, 1380–1700 kPa). Fig. 2b shows a strong correlation between e_{cs} and e_{min} for glass beads at three different stress levels (i.e., p' = 120–145, 250–275, 498–578 kPa). The strong correlation between minimum void ratio and the critical state void ratio for granular material is also supported by the work in Chang and Meidani (2013), and Torres-Cruz et al. (2017). Thus, we hypothesize that the change of critical state void ratio with respect to GSD is caused by the same particle mix mechanism that influences the change of minimum void ratio with respect to GSD.

In this paper, based on this hypothesis, we aim to extend the particle packing model for minimum void ratios (Chang et al., 2017) to a new model for the prediction of critical state void ratios.

3. Development of a model for e_{cs}

3.1. A simplified particle packing model for e_{min}

A simplified version of the particle packing model for predicting minimum void ratio considering the effect of GSD (Chang et al., 2017) is briefly summarized in the Appendixes A and B. The simplified model can be represented by a function:

$$e_{min} = F(\bar{e}_{min}, \Psi, s, t) \quad (1)$$

On the right-hand side of Eq. (1), $\bar{e}_{min}$ is the minimum void ratio for a

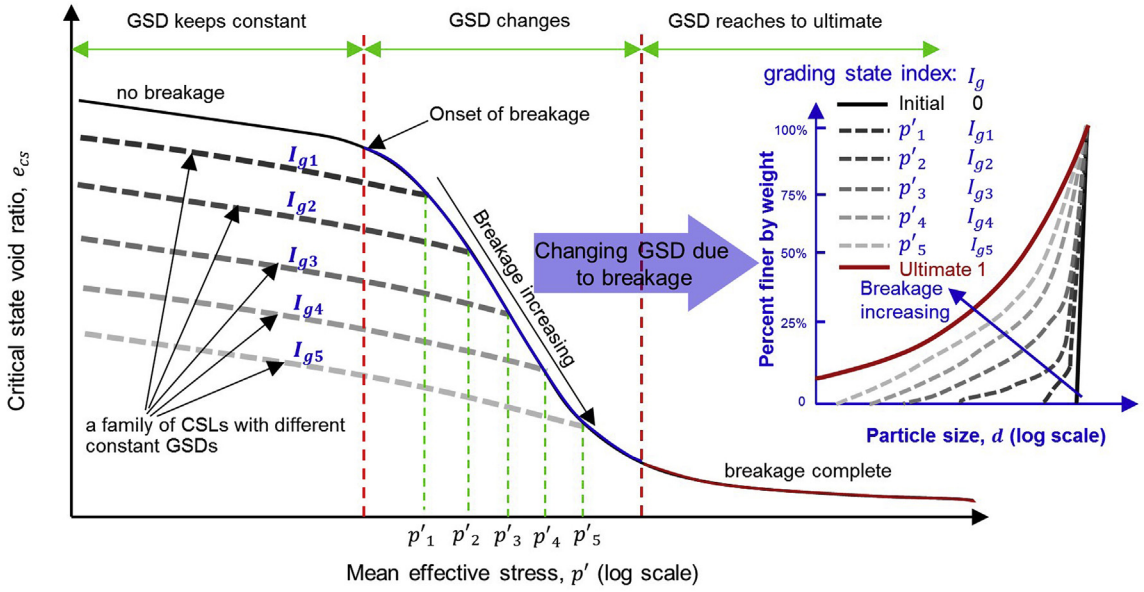

Fig. 1. Three-segment critical state line.

mono-sized packing, which is assumed to be a constant, independent of particle size; parameters s and t are material properties of the granular soil, independent of the GSD. On the left-hand side of Eq. (1), e_{min} is the minimum void ratio of a packing of granular soil with any GSD (denoted as Ψ), which can be obtained from the following input variables: $\bar{e}_{min}$, the parameters s and t, and the GSD (Ψ) of a granular soil. The value of $\bar{e}_{min}$ can be directly obtained from the measured e_{min} data on uniformly graded samples. The model parameters, s and t, can be experimentally calibrated from the data for e_{min} of two samples with two different GSDs. The procedure of determining these two parameters is illustrated in Chang et al. (2017).

Experimental tests on quartz silty sand (Papadopoulou and Tika, 2008) and glass beads (Li, 2013; Li et al., 2015) were used to validate the simplified model for e_{min}. Their grain size distributions are shown by gradation curves in Fig. 3a and b. The mono-sized packing $\bar{e}_{min}$ and the calibrated two parameters s and t for glass beads and quartz silty sand are listed in Table 1.

The predictions using the model are given in Fig. 4. Comparison of the predicted and measured results shows a good agreement.

3.2. Extension of the particle packing model to e_{cs}

The particle packing model for minimum void ratio in the previous section can be extended to critical state void ratio by replacing minimum void ratio e_{min} with critical state void ratio $e_{cs}(p')$ under a specified mean effective stress p'. Thus, the function of Eq. (1) can be written as,

$$e_{cs}(p') = F(\bar{e}_{cs}(p'), \Psi(p'), s, t) \quad (2)$$

On the right-hand side of Eq. (2), $\Psi(p')$ is the GSD of the granular soil at critical state under the mean effective stress p', $\bar{e}_{cs}(p')$ is the critical state void ratio of a mono-sized particle packing under the mean effective stress p'. We used the same assumption in the model described in last section that $\bar{e}_{cs}(p')$ is independent of particle size. Parameters s and t are material properties of the granular soil, independent of the GSD.

It is noted that $e_{cs}(p')$ and $\bar{e}_{cs}(p')$ represent the CSL of a multi-sized particle packing and a mono-sized particle packing respectively. Thus, Eq. (2) shows that the CSL of a multi-sized granular material can be predicted from the CSL of a mono-sized packing. Regarding the variable $\Psi(p')$, two cases are considered in this study:

(1) Case I: no particle breakage occurs at critical states in the range of p'. Thus, the GSDs of the material at critical state under various p' maintain same and are independent of p' (i.e. $\psi(p') = \psi$). In this case, Eq. (2) can be reduced to the following equation.

$$e_{cs}(p') = F(\bar{e}_{cs}(p'), \Psi, s, t) \quad (3)$$

(2) Case II: particle breakage occurs at critical states in the range of p'. In this case, GSD is function of p' (i.e. $\Psi(p')$).

In the following two sections, the proposed model for predicting CSL will be verified for these two cases.

4. Model application to CSL with constant GSD (no breakage)

In this section, four sets of experimental results obtained from the literature were used to validate the proposed model. These four sets of triaxial test results were reported by: Papadopoulou and Tika (2008) on quartz silty sand, Nguyen et al. (2017) on Camargue silty sand, and Li et al. (2015) on glass beads and on DEM simulation.

These four sets of experimental results satisfy the condition of Case I (constant GSD). For quartz silty sand and glass beads, Papadopoulou and Tika (2008) and Li et al. (2015) indicated that no particle breakage occurred in their triaxial tests and stated that the same GSD are maintained before and after tests. For DEM simulation, particle breakage was not considered (Li et al., 2015). For Camargue silty sand, although Nguyen et al. (2017) did not specifically mention about particle breakage, we assume that particle breakage is negligible because the maximum p' in the tests was 700 kPa, while particle breakage does not occur for quartz uniform sand until p' is greater than 1 MPa, according to the study by Been et al. (1991).

4.1. Measured CSL for four materials without effect of particle breakage

The gradation curves of specimens are presented in Fig. 3 for quartz silty sand and glass beads, and in Fig. 5 for DEM simulation and Camargue silty sand. Experimental data on CSL are presented in Fig. 6a for quartz silty sand, in Fig. 6b for Camargue silty sand, in Fig. 6c for glass beads and in Fig. 6d for DEM simulation. Each CSL corresponds to a gradation curve shown in Fig. 3 or Fig. 5. The measured e_{cs} on quartz silty sand and Camargue silty sand were obtained under both undrained and drained conditions under a range of confining pressure. The measured e_{cs} on glass beads and DEM simulation were obtained under the drained condition under several different confining pressures. Thus, there are many stress level points in Fig. 6a and b while there are only a few stress

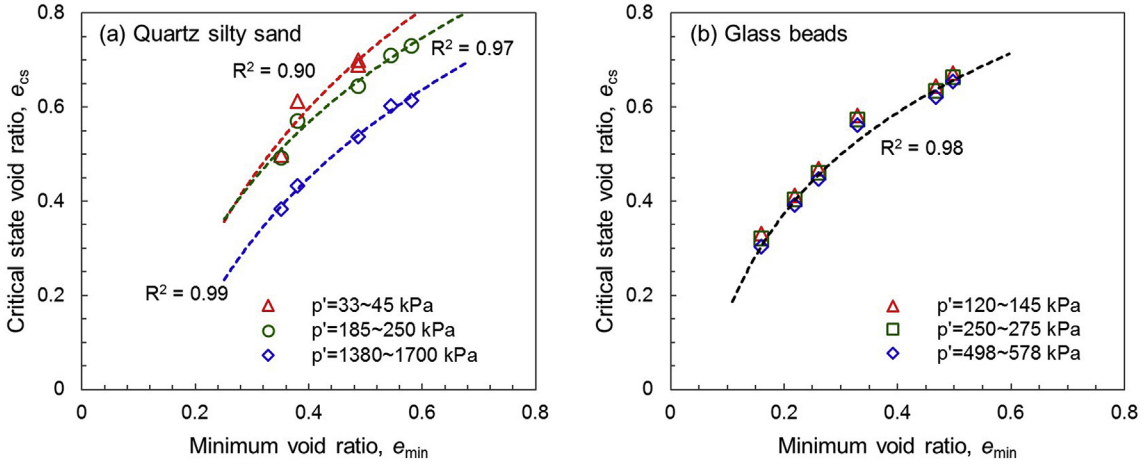

Fig. 2. The correlation between minimum void ratio and critical state void ratio: (a) quartz silty sand (data from Papadopoulou and Tika (2008)) and (b) glass beads (data from Li (2013)).

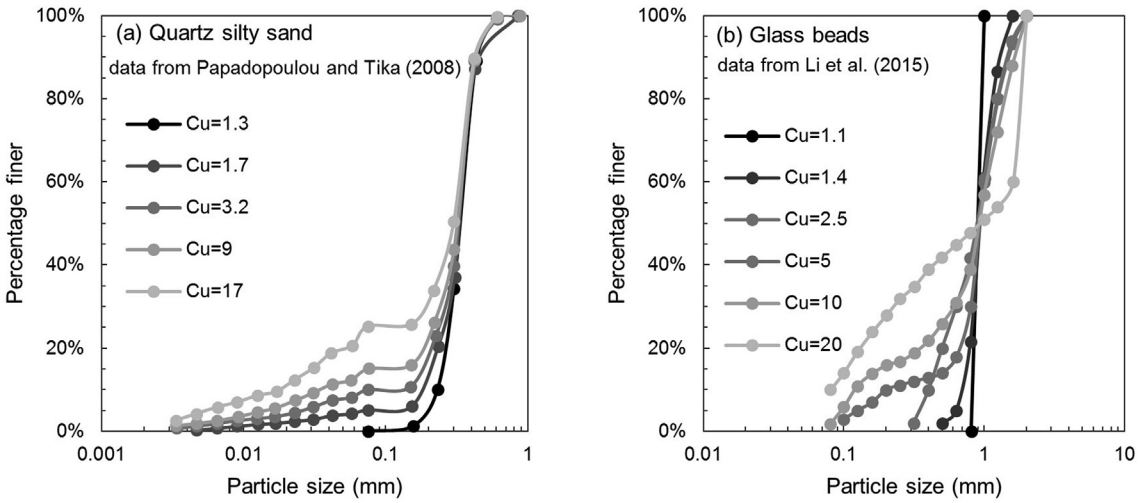

Fig. 3. The gradation of (a) quartz silty sand, and (b) glass beads.

Table 1
Input parameters for glass beads and quartz silty sand.

Soil type	Ref.	$\bar{e}_{min}$	s	t
Glass beads	Li (2013)	0.445	2.3	2.2
Quartz silty sand	Papadopoulou and Tika (2008)	0.585	5.0	4.0

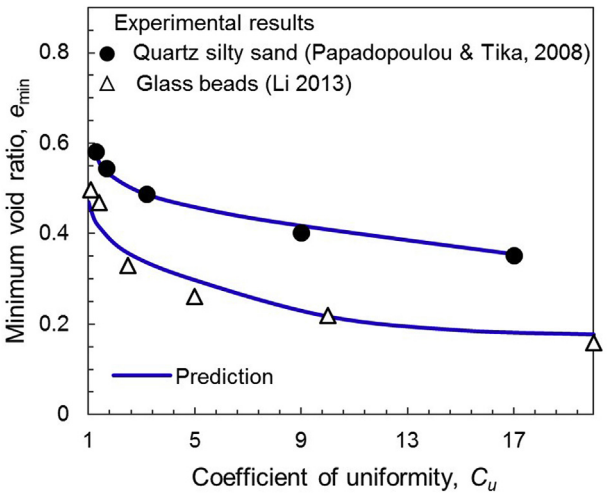

Fig. 4. The comparison between predicted and measured minimum void ratios for quartz silty sand and glass beads.

level points in Fig. 6c and d.

4.2. Model prediction of CSL

The model (Eq. (3)) requires three types of input data, i.e., the mono-sized CSL ($\bar{e}_{cs}(p')$), parameters s and t, and GSD (Ψ).

(1) Grain size distribution

GSD is usually expressed in terms of gradation curve. The gradation curves for these four materials (in Figs. 3 and 5) can be converted to GSD in the way illustrated in Appendix B.

(2) Determination of $\bar{e}_{cs}(p')$, s and t

The function $\bar{e}_{cs}(p')$ is the CSL for a mono-sized packing, which can be obtained from triaxial tests on uniformly graded granular material. An empirical expression for CSL proposed by Li and Wang (1998) was used to fit the mono-sized CSL:

$$\bar{e}_{cs}(p') = \bar{e}_{ref} - \bar{\lambda}\left(\frac{p'}{p_{atm}}\right)^{\bar{\xi}} \quad (4)$$

where $\bar{e}_{ref}$ is the intercept of CSL on e-axis corresponding to a mean effective stress $p' = 0$; $\bar{\lambda}$ and $\bar{\xi}$ are two parameters controls the curve shape of CSL in the $e-\log p'$ plane; $p_{atm} = 101.3$ kPa. To differentiate mono-sized packing from multi-sized packing, the overbar " – " is used for the parameters associated to mono-sized packing.

It is noted that two other types of formulas can also be used for the expression of a mono-sized CSL (see Appendix A (Eq. (A.9) and Eq. (A.11)). Herein, Eq. (4) is used.

For each material, the critical state parameters ($\bar{e}_{ref}$, $\bar{\lambda}$, $\bar{\xi}$) for the mono-sized CSL were obtained by fitting Eq. (4) to the experimental CSL data in Fig. 6 (i.e., coefficient of uniformity $C_u = 1.3$, 2.05, 1.1 and 1.0 were used for quartz silty sand, Camargue silty sand, glass beads and DEM simulation, respectively). These fitted mono-sized critical state parameters for each material are listed in Table 2.

The two model parameters s and t were then calibrated from the data for critical state void ratios of samples with two different GSDs using the same procedure described by Chang et al. (2017). The two model parameters s and t for these four materials are listed in Table 2.

Note that the values of parameters s and t obtained from test data of critical state void ratios for glass beads and quartz silty-sand listed in Table 2 are identical to the values of parameters s and t obtained from test data of minimum void ratio listed in Table 1.

(3) Predicted CSL for various GSD

For each material, using the parameters listed in Table 2, the CSL for each GSD can be predicted by using Eq. (3). The predicted CSL in the $e_{cs} - \log p'$ plane for each GSD is presented in Fig. 6a for quartz silty sand, in Fig. 6b for Camargue silty sand, in Fig. 6c for glass beads, and in Fig. 6d for DEM simulation. The CSL moves downward with increasing coefficient of uniformity (C_u). The comparison between the predicted and measured results on these four materials shows a good agreement.

Fig. 7 shows the critical state void ratios at three stress levels for various C_u. The data points were interpreted from experimental results in Fig. 6a for quartz silty sand and in Fig. 6c for glass beads. The minimum void ratio are also plotted in Fig. 7a for quartz silty sand and Fig. 7b for glass beads to show the influence of C_u on the minimum void ratio and

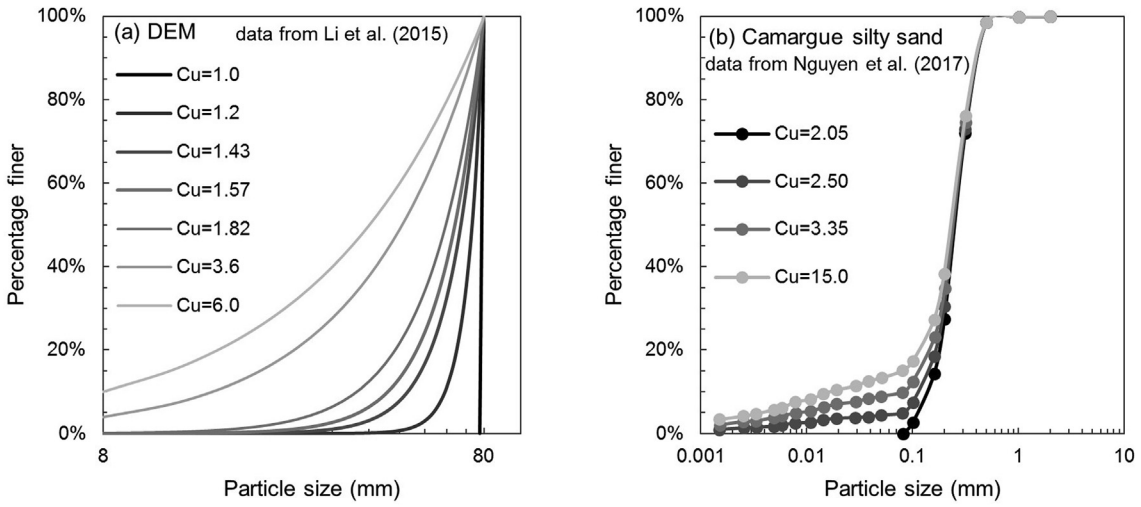

Fig. 5. The gradation of (a) DEM simulation, and (b) Camargue silty sand.

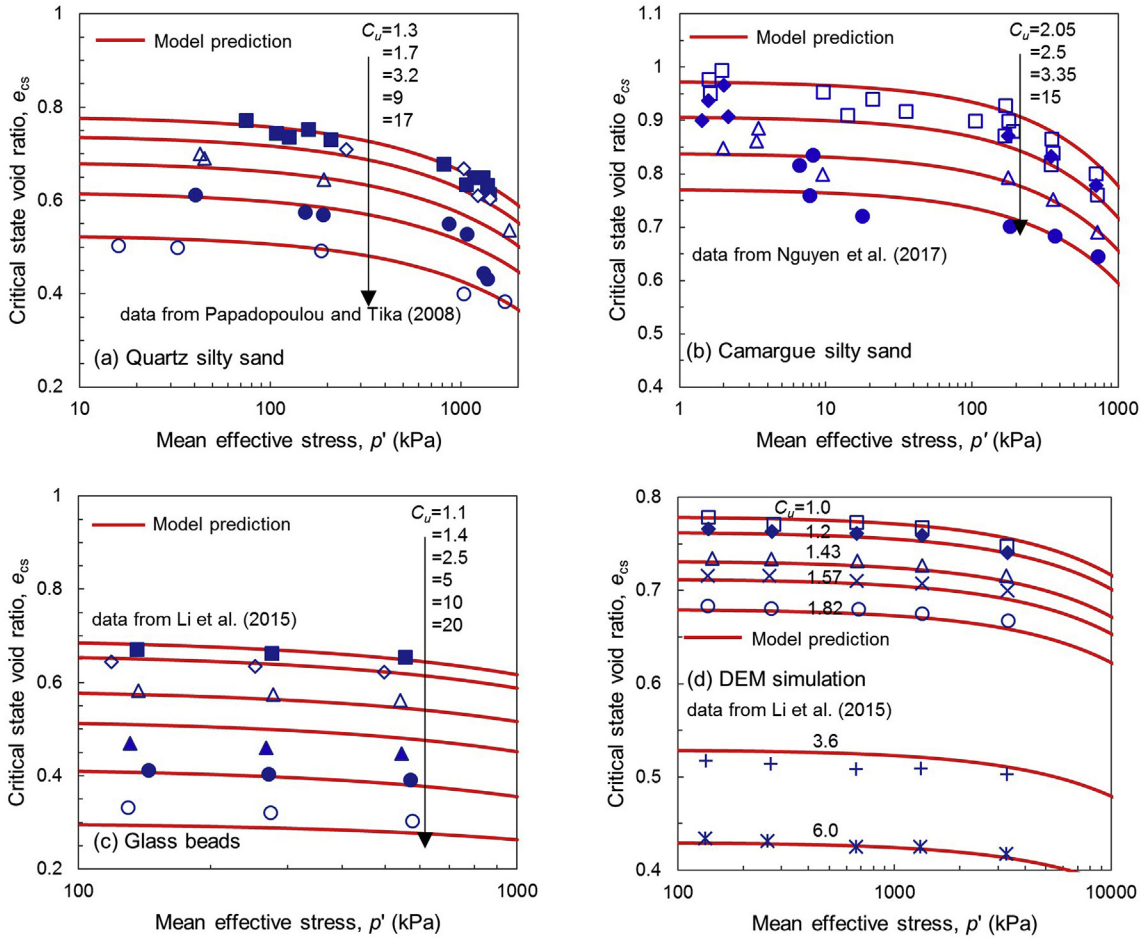

Fig. 6. Comparison between measured and predicted critical void ratios: (a) quartz silty sand, (b) Camargue silty sand, (c) glass beads, and (d) DEM simulation.

the critical state void ratio. The predicted results are in a good agreement with the test results from experiments. The comparison also demonstrates the validity of the proposed model.

Observed from Fig. 7, the influence of C_u on the critical void ratio is in the same manner as that on the minimum void ratio. Note that the critical state void ratios were predicted using the same values of parameters s and t for minimum void ratio. This indicates that critical state void ratio is influenced by GSD with the same mechanisms that influence minimum void ratios.

4.3. Discussion

It is noted that the form of Eq. (4), with critical state parameters, e_{ref}, λ and ξ, is also used for multi-sized packing. According to the derivation

Table 2
Input parameters for four types of granular materials.

Material type	Ref.	$\bar{e}_{min}$	Eq. (4)			s	t
			$\bar{e}_{ref}$	$\bar{\lambda}$	$\bar{\xi}$		
Glass beads	Li (2013), Li et al. (2015)	0.445	0.695	0.01	0.9	2.3	2.2
DEM	Li et al. (2015)	–	0.778	0.0012	0.9	1.8	1.8
Quartz silty sand	Papadopoulou and Tika (2008)	0.585	0.79	0.024	0.7	5.0	4.0
Camargue silty sand	Nguyen et al. (2017)	–	0.99	0.04	0.7	7.0	3.5

in Appendix A, the value of λ is dependent on GSD, thus is not same for all CSLs obtained from a type of soils with different gradation. Therefore, theoretically, the CSLs are not parallel, which opposes the commonly used assumptions (e.g. Verdugo and Ishihara, 1996; Konrad, 1998). We plot the predicted λ versus C_u in Fig. 8a and e_{ref} versus C_u in Fig. 8b. These two figures show that both e_{ref} and λ decrease with an increase of C_u. The same trend were found by Bandini and Coop (2011), Li et al. (2015), and Xiao et al. (2015).

Here, we intend to show that the proposed model is capable to predict CSL based on the GSD. The predictions of CSL for these four sets of experimental tests were repeated in Appendix C, using the logarithmic formula in Eq. (A.9) and the sigmoid formula in Eq. (A.11) respectively. The comparison between the predicted results and the test results from experiments shows a good agreement.

5. Model application to CSL with GSD changing due to particle breakage

In this section, the applicability of this proposed model under the condition of Case II in section 3.2 is to be validated. Thus, it is required to use a set of experimental results of CSL with particle breakage, and with measured evolution of GSD with respect to p'. For this purpose, the set of experimental results reported on Tacheng rockfill material by Xiao et al. (2016b) was selected to verify the model on the condition of Case II.

5.1. Measured CSL for the rockfill material with effect of particle breakage

The rockfill material is classified as well-graded gravel according to ASTM D 2487-06 (2006) and its initial gradation is shown in Fig. 9a. The specimens were prepared by compacting into four different initial void ratios (e_0 = 0.189, 0.244, 0.285, 0.317). The specimens were then sheared to critical state under drained triaxial conditions at four different confining stresses (p_0= 0.2, 0.4, 0.8, 1.6 MPa). The measured CSLs of the rockfill material for the four different initial void ratios are plotted in the $e - \log p$' plane as shown in Fig. 9b. Corresponding to each data point in Fig. 9b, the gradation curves were measured.

Xiao et al. (2016b) used Talbot equation to express the gradation of a specimen for the rockfill material as follows:

$$F(d) = \left(\frac{d}{d_M}\right)^{3-\alpha} \tag{5}$$

where d_M is the maximum particle diameter and α is a fractal dimension. For this rockfill material, d_M is 60 mm. The fractal dimension is denoted as α_0 for the initial gradation, α_c for the gradation at critical state and α_u for the ultimate gradation. The initial gradations for all specimens were same as shown in Fig. 9a ($\alpha_0 = 0.21$). The ultimate fractal dimension $\alpha_u = 2.69$ for the rockfill material (Xiao et al., 2016b). The gradation at critical state (at end of shearing) α_c for various tests are listed in Table 3. For a given initial void ratio (e.g., $e_0 = 0.244$), the critical state fractal dimension α_c increases with the increasing of confining pressure as shown in Fig. 9a.

It is noted that the gradations of samples are different for the four initial void ratios due to particle breakage resulting from compaction during the sample preparation. Thus, the CSLs are different for each initial void ratio.

Table 3 lists the test results of gradations at critical state for all specimens. The experimental results in Table 3 shows that, under the same p_0, smaller e_0 has more breakage (i.e. larger α_c).

Xiao et al. (2016b) interpreted five CSLs with five constant GSDs from their systematic experimental results on Tacheng rockfill material. The interpreted five CSLs were obtained by connecting the critical state points with same GSD (i.e. with same α_c). These five CSLs (with same α_c) are plotted in solid line as shown in Fig. 10a. The five GSDs corresponding to these five CSLs are shown in Fig. 10b in terms of gradation curve.

5.2. Model parameters and GSD evolution

(1) Determination of $\bar{e}_{ref}, \bar{\lambda}, \bar{\xi}, s$ and t

The model requires the following parameters: the mono-sized critical state parameters ($\bar{e}_{ref}, \bar{\lambda}, \bar{\xi}$) and the two model parameters (s and t). The mono-sized critical state parameters ($\bar{e}_{ref}, \bar{\lambda}, \bar{\xi}$) are usually obtained directly from the experimental results on CSL of uniformly graded sample without particle breakage. However, for Tacheng rockfill material, this

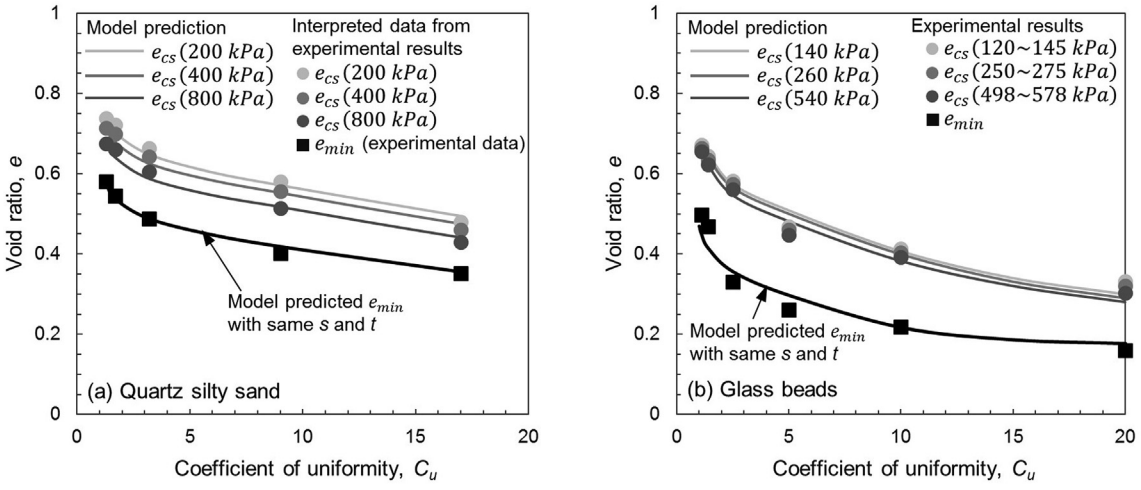

Fig. 7. The predicted results and interpreted data points from experimental results for both critical state void ratio and minimum void ratio with respect to coefficient of uniformity C_u: (a) quartz silty sand, and (b) glass beads.

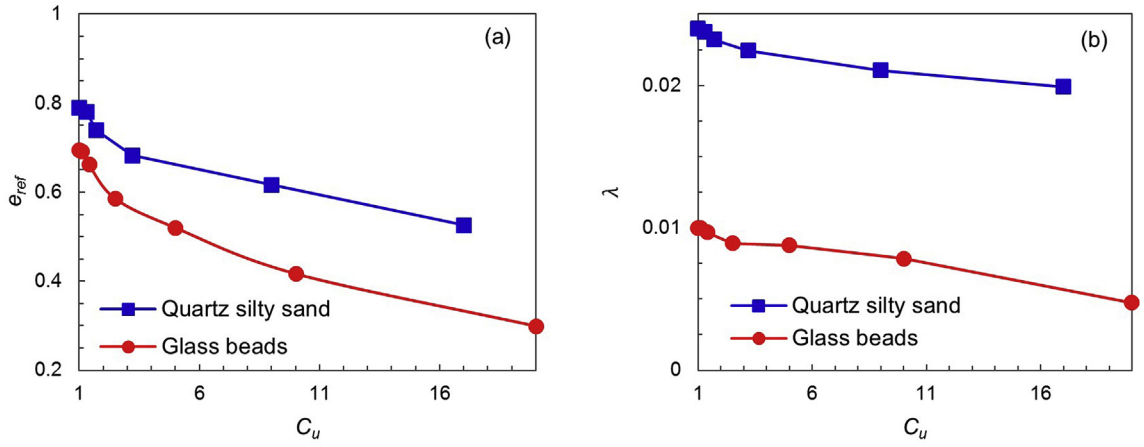

Fig. 8. Relationships between (a) e_{ref} and C_u, and (b) λ and C_u.

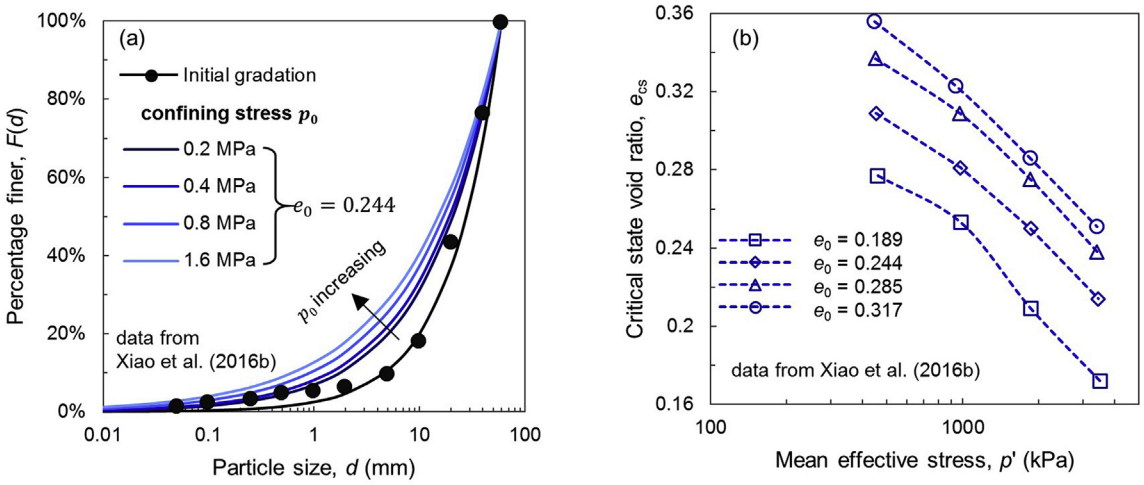

Fig. 9. (a) Gradation curves and (b) the measured CSLs of the rockfill material at various initial void ratios and confining stresses.

Table 3
Test results of large-scale triaxial compression on the rockfill material (data obtained from Xiao et al., 2016b).

e_0	p_0 (MPa)	p' (MPa)	e_{cs}	α_c
0.189	0.2	0.46	0.277	2.41
	0.4	0.983	0.253	2.453
	0.8	1.863	0.209	2.514
	1.6	3.503	0.172	2.557
0.244	0.2	0.453	0.309	2.35
	0.4	0.98	0.281	2.39
	0.8	1.86	0.25	2.45
	1.6	3.453	0.214	2.496
0.285	0.2	0.45	0.337	2.29
	0.4	0.973	0.309	2.35
	0.8	1.857	0.275	2.4
	1.6	3.41	0.238	2.452
0.317	0.2	0.447	0.356	2.245
	0.4	0.94	0.323	2.33
	0.8	1.853	0.286	2.35
	1.6	3.407	0.251	2.403

type of experimental data is not available. Therefore, using Eq. (3), the mono-sized critical state parameters ($\bar{e}_{ref}, \bar{\lambda}, \bar{\xi}$) and the two model parameters (s and t) are obtained by back-fitting the five CSLs for constant GSDs available for Tacheng rockfill material as shown in Fig. 10a (the back fitting process required at least 2 CSLs for constant GSDs). The back fitted mono-sized critical state parameters and two model parameters (s and t) are listed in Table 4. The back fitted mono-sized CSL of Tacheng rockfill material is plotted in Fig. 11.

Using the input parameters in Table 4, the predictions for the five CSLs are shown in Fig. 11 in blue dashed lines. The predicted results are in good agreement with the interpreted results from experimental data.

(2) The evolution of GSD – p' at critical state $\Psi(p')$

In order to predict the CSL using Eq. (2) considering the evolution of GSD due to particle breakage, the model requires the function $\Psi(p')$, i.e., the evolution of GSD with respect to p' at critical state. The function $\Psi(p')$ measured from experiments is used as an input in the following analysis.

Since the GSD for the rockfill material is represented by Talbot equation (Eq. (5)), $\Psi(p')$ can be obtained by $\alpha_c(p')$. Xiao et al. (2016b) suggested a form of the fractal dimension α_c of gradation at critical state as a function of initial void ratio e_0 and confining stress p_0, i.e. $\alpha_c(p_0, e_0)$, given by:

$$\alpha_c = \alpha_{eo} - \chi_a e_0 + \kappa_a log\frac{p_0}{p_{atm}} \quad (6)$$

where, α_{eo}, χ_a and κ_a are parameters. Xiao et al. (2016b) determined these parameters by fitting the experimental data: $\alpha_{eo} = 2.57, \chi_a = 1.16$, $\kappa_a = 0.173$.

Since the tests performed by Xiao et al. (2016b) were drained triaxial tests, the mean effective stress p' can be determined by the confining

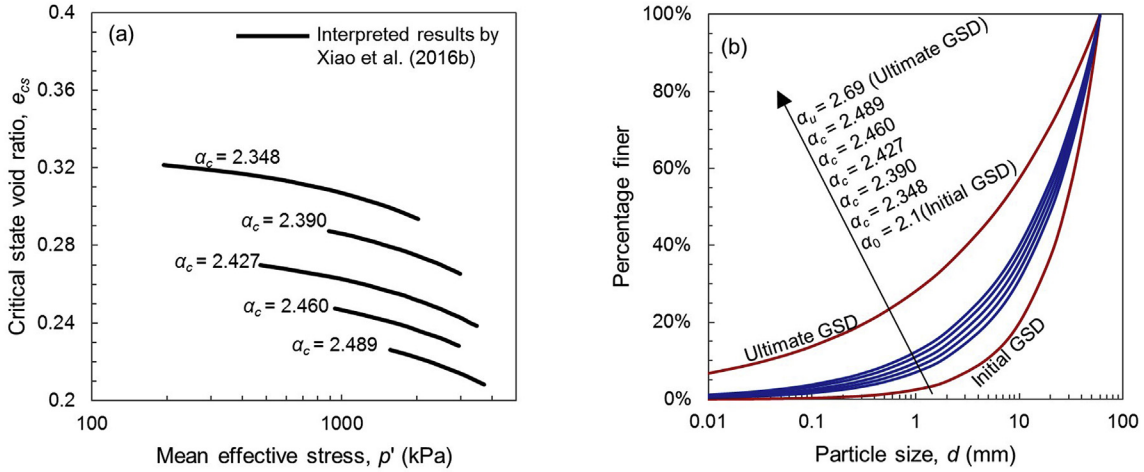

Fig. 10. (a) Five CSLs for constant GSD and (b) the corresponding five gradation curves.

Table 4
Input parameters for Tacheng rockfill material.

$\bar{e}_{ref}$	$\bar{\lambda}$	$\bar{\xi}$	s	t	M
0.549	0.0048	0.7	7	2.5	1.64

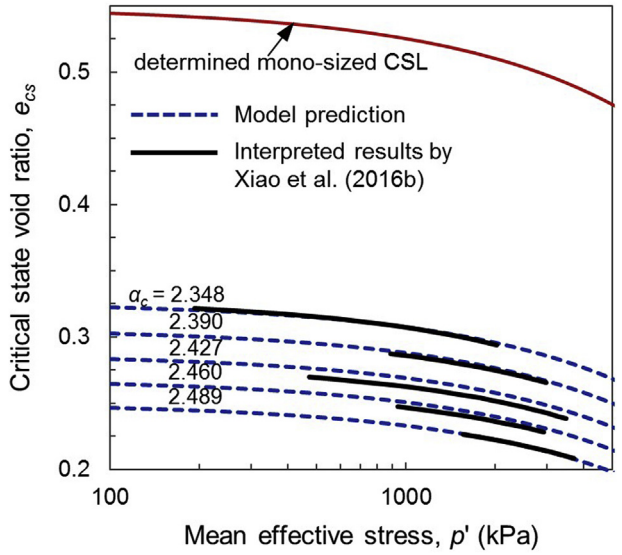

Fig. 11. The determined mono-sized CSL of Tacheng rockfill material and predicted CSLs for constant GSD.

stress p_0 as following:

$$p^{'} = \left[\left(\frac{3+2M}{3-M}\right)+2\right]\cdot\frac{p_0}{3} \tag{7}$$

where M is the stress ratio at critical state. Xiao et al. (2016b) found that $M = 1.64$ for Tacheng rockfill material under all test conditions.

By substituting Eq. (7) into Eq. (6), the function $\alpha_c(p^{'})$ for Tacheng rockfill material can be obtained, given by

$$\alpha_c = 2.57 - 1.16e_0 + 0.173\log\frac{p^{'}}{2.206p_{atm}} \tag{8}$$

Eq. (8) is plotted in Fig. 12. Fig. 12 shows that Eq. (8) is in good agreement with the measured results from Xiao et al. (2016b). With Eq. (8), $\Psi(p^{'})$ can be obtained by substituting α_c into Eq. (5).

It is noted that for loading conditions different from the conventional triaxial condition, Ψ may not be only a function of mean effective stress $p^{'}$. For example, Ψ may be dependent on factors of repeated loading conditions or intermediate principle stress ratio (Xiao et al., 2016a). In order to model the CSL due to particle breakage, the GSDs at critical state under the specific types of loading conditions, such as repeated loading, need to be measured, which will be the required input into the model. In this paper, only conventional triaxial conditions are considered, thus Ψ is considered to be only a function of mean effective stress $p^{'}$.

5.3. Model prediction of CSL for the rockfill material with effect of particle breakage

Inputting the parameters in Table 4 and $\Psi(p^{'})$ into the model (Eq. (2)), the CSL for Tacheng rockfill material with effect of particle breakage was predicted and plotted in Fig. 13. It is noted that $\Psi(p^{'})$ are different for the specimens with different initial void ratios, thus the predicted CSLs are different for different initial void ratios. It is also noted that the predicted CSLs in Fig. 13 represent only the second segment of the CSL in Fig. 1. The model predicted results are in good agreement with the experimental results.

6. Conclusions

Experimental results show that grain size distribution (GSD) has a

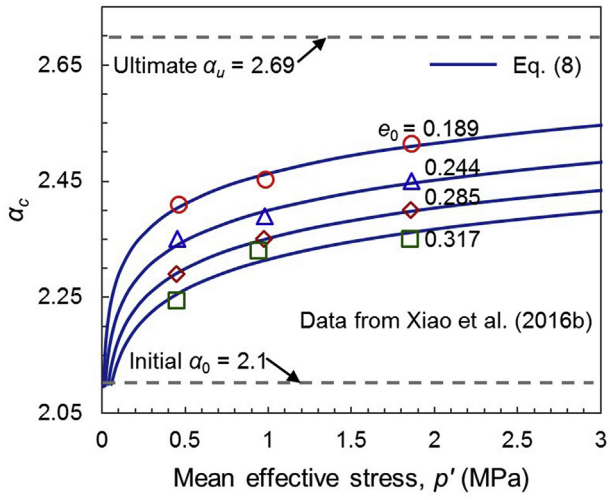

Fig. 12. The fractal dimension α_c of gradation at critical state for Tacheng rockfill material under various mean effective stresses.

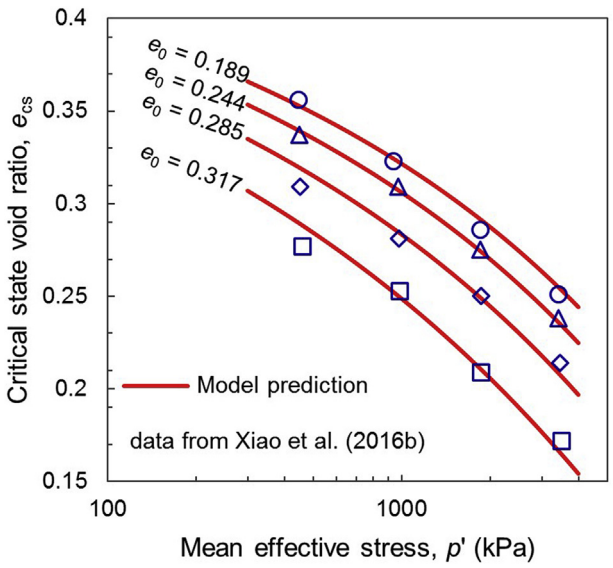

Fig. 13. The CSL with GSD evolution due to particle breakage.

significant influence on CSL. However, there are no analytical models available for determining CSL by directly considering GSD. This paper presents an analytical model for determining the CSL of granular materials with influence of GSD based on the particle packing model. The following conclusions can be drawn from this study.

(1) The particle packing model for minimum void ratio proposed by Chang et al. (2017) was extended to predict critical state void ratio directly from GSD based on the hypothesis that the variation of critical state void ratio with respect to GSD is caused by the same particle mixing mechanism that influences the variation of minimum void ratio. The experimental and predicted results indicated that this hypothesis is plausible.
(2) The proposed model can predict the CSL of a multi-sized particle packing based on the CSL of a mono-sized packing. The CSL of a mono-sized packing can be characterized by 2 or 3 critical state parameters shown in Eq. (4). The mono-sized critical state parameters can be obtained by fitting the critical state data on a uniformly graded granular material using Eq. (4).
(3) The proposed model requires two material parameters (s and t) and mono-sized critical state parameters. It was found that the same material parameters (s and t) can be used for predicting both minimum and critical state void ratios of granular materials with various gradations. Thus, these two material parameters (s and t) can be calibrated from the data for either minimum or critical state void ratios of samples.
(4) The model was evaluated by experimental data on four types of granular materials. The comparisons between predicted and measured results have demonstrated that the proposed model is capable of predicting the CSL of a multi-sized packing from the CSL of a mono-sized packing.
(5) In this study, it is derived in Appendix A that both e_{ref} and λ in Eq. (A.8) or (A.9) depend on GSD of material. The model mathematically shows that both e_{ref} and λ decrease with an increase of C_u, which agrees with experimental observations (Bandini and Coop, 2011; Li et al., 2015; Xiao et al., 2016b).
(6) The particle breakage influence on CSL is caused mainly by the evolution of GSD. In this study, the evolution of GSD at critical state in relation to p' is known in advance. By incorporating the known relation $\Psi(p')$, CSL was predicted with influence of particle breakage. The proposed model is evaluated by the experimental results on Tacheng rockfill material to illustrate the applicability of the model in determining CSL for granular material with particle breakage. The predicted CSLs show a good agreement with the experimental results. Note that the function $\Psi(p')$ used in the prediction is exclusive for Tacheng rockfill material. For other granular material, this relation needs to be studied.

This proposed model has potential applicability in the analysis of liquefaction for silty sand. The model is also useful in the study for the degradation of strength and settlement for granular materials due to particle breakage in a high earth dam.

Acknowledgement

This work was supported by the National Science Foundation of the United States under a research grant (CMMI-1917238). The support is greatly acknowledged.

Appendix A. A Simple Particle Packing Model

Grain size distribution (GSD) of soil is usually represented by a gradation curve. A continuous gradation curve can be discretized into n size-classes of particles (shown in Appendix B), and the GSD of a multi-sized packing can be characterized by: solid fraction y_i for each size-class of particles with particle size d_i, i.e. $\{d_i, y_i, i = 1,\ldots, n\}$. Note that the particle size is sorted by $d_1 > d_2 > \ldots > d_n$. The detailed process of discretization is given in Appendix B.

In the particle packing model proposed by Chang et al. (2017), the minimum void ratio of a multi-sized packing can be expressed as:

$$e_i^M = \sum_{j=1}^{n} \left(e_j - a_{ij}(1 + e_j) - b_{ij} e_j\right) y_j \tag{A.1}$$

where e_i^M is the minimum void ratio of the multi-sized packing assuming that the i-th size-class of particles is dominant; the subscript i is the dominant size-class of particles for the mixture; e_j is the minimum void ratio of a packing that contains only the j-th size-class of particles d_j; y_j is the solid volume fraction of the j-th size-class of particles; the filling-mechanism coefficient a_{ij} and the embedment-mechanism coefficient b_{ij} are determined by the following function:

$$a_{ij} = \begin{cases} \left(1 - \dfrac{d_j}{d_i}\right)^s & for \;\; d_i > d_j \\ 0 & for \;\; d_i \le d_j \end{cases} \tag{A.2}$$

$$b_{ij} = \begin{cases} \left(1 - \dfrac{d_i}{d_j}\right)^t & for \;\; d_i < d_j \\ 0 & for \;\; d_i \geq d_j \end{cases} \tag{A.3}$$

Parameters s and t are material properties of the granular soil, independent of the GSD.

This model was developed based on the mix mechanism. In consideration of the mix mechanism, a dominant particle size d_i is selected. The packing containing particles of single size d_i is regarded as the base packing, which is used for building up the multi-sized particle packing. The particles with sizes smaller than the dominant particle size (i.e., d_i) are regarded as fillers into the voids of the base packing, whereas the particles with sizes greater than the dominant particle size are regarded as inclusions embedded in the base packing.

Observed from the study of geological fault gouges, Sammis et al. (1987) found that the shapes of fractured smaller particles are similar in a fractal manner to the shapes of unfractured large particles. This conclusion is supported by the experiments on crushed Basalt by Youd (1973) and by the experiments on Huston sand by Li et al. (2015). Thus, for breakage material, the particle shape is independent of particle size. Consequently, we may assume that the minimum void ratio for a mono-sized packing (i.e. the coefficient of uniformity $C_u = 1$) is a constant for any particle size, i.e. $e_j = \overline{e}$ ($j = 1, \ldots, n$).

Based on this assumption, a simplified particle packing model is derived for breakage material. Eq. (A.1) becomes:

$$e_i^M = \alpha_i \overline{e} - \beta_i \tag{A.4}$$

where

$$\alpha_i = 1 - \sum_{j=1}^{n} (b_{ij} + a_{ij}) y_j; \qquad \beta_i = \sum_{j=1}^{n} a_{ij} y_j \tag{A.5}$$

The dominant class of particles is not known in priori. Since the dominant class of particles is one of the size-classes of particles, there are n possible trial values for the dominant size, and n trial values of e_i^M can be computed by Eqs. (A.4 and A.5). The true minimum void ratio of the multi-sized packing can be determined by the following equation:

$$e^M = \max\left\{e_i^M, i = 1, \ldots, n\right\} \tag{A.6}$$

The particle packing model described above is for the prediction of minimum void ratio. However, it can be extended for the prediction of critical state void ratio by treating the variable e as critical state void ratio. Thus, e_i^M is the critical state void ratio of the multi-sized packing assuming that the i-th size-class of particles is dominant; $\overline{e}$ is the critical state void ratio of a mono-size packing; e^M is the true critical state void ratio of the multi-sized packing. The model can be summarized by Eqs. (A.4), (A.5) and (A.6). The required input data are $\overline{e}_{cs}$, GSD, s, t. Thus, we need to know the equation of CSL of the mono-sized packing in order to determine the value of $\overline{e}_{cs}$ for a given mean effective stress.

After the equation of CSL of the mono-sized packing is known, the equation of CSL of a packing with any constant GSD can be derived from this model. Considering the expression of CSL by three different formulas:

(1) power formula proposed by Li and Wang (1998)

The equation of CSL for a mono-size packing and for a packing with any constant GSD are given below:

$$e_{cs} = e_{ref} - \lambda \left(\frac{p'}{p_{atm}}\right)^{\xi}; \qquad \overline{e}_{cs} = \overline{e}_{ref} - \overline{\lambda} \left(\frac{p'}{p_{atm}}\right)^{\overline{\xi}} \tag{A.7}$$

where e_{ref} is the intercept of CSL on e-axis corresponding to a mean effective stress $p' = 0$; λ and ξ are two parameters controls the curve shape of CSL in the $e - \log p'$ plane; $p_{atm} = 101.3$ kPa. $\overline{e}_{ref}, \overline{\lambda}, \overline{\xi}$ are mono-sized critical state parameters. For distinguish from multi-sized packing, the overbar " – " refers to the parameter for mono-sized packing.

Substituting Eq. (A.7) into Eq. (A.4), it leads to:

$$e_{ref} = \alpha_i \overline{e}_{ref} - \beta_i; \quad \lambda = \alpha_i \overline{\lambda}; \quad \xi = \overline{\xi} \tag{A.8}$$

(2) logarithmic formula

The equation of CSL for a mono-size packing and for a packing with any constant GSD are given below:

$$e_{cs} = e_{ref} - \lambda log\left(\frac{p'}{p_{atm}}\right); \qquad \overline{e}_{cs} = \overline{e}_{ref} - \overline{\lambda} log\left(\frac{p'}{p_{atm}}\right) \tag{A.9}$$

where e_{ref} is a reference void ratio corresponding to a mean effective stress $p' = p_{atm} = 101.3$ kPa, λ is the slope of the CSL in the $e - \log p'$ plane.

Substituting Eq. (A.9) into Eq. (A.4), it leads to:

$$e_{ref} = \alpha_i \overline{e}_{ref} - \beta_i; \quad \lambda = \alpha_i \overline{\lambda} \tag{A.10}$$

(3) Sigmoid formula proposed by Gudehus (1997)

The equation of CSL for a mono-size packing and for a packing with any constant GSD are given below:

$$e_{cs} = e_{cu} + (e_{cmax} - e_{cu})exp\left[-\left(\frac{p'}{mp_{atm}}\right)^{\xi}\right]; \quad \overline{e}_{cs} = \overline{e}_{cu} + \left(\overline{e}_{cmax} - \overline{e}_{cu}\right)exp\left[-\left(\frac{p'}{\overline{m}p_{atm}}\right)^{\overline{\xi}}\right] \tag{A.11}$$

where e_{cu} is critical void ratio when p' = infinity; e_{cmax} is critical void ratio when p' = 0; m and ξ are two parameters controls the curve shape of CSL in the e – log p' plane.

Substituting Eq. (A.11) into Eq. (A.4), it leads to:

$$e_{cu} = \alpha_i \overline{e}_{cu} - \beta_i; \quad e_{cmax} = \alpha_i \overline{e}_{cmax} - \beta_i; \quad m = \overline{m}; \quad \xi = \overline{\xi} \tag{A.12}$$

Appendix B. Discretization of a continuous gradation

In this Appendix, a discretization process is described for a continuous gradation curve. As an example, the gradation curve is shown in Fig. B.1. The vertical axis is percent finer and the horizontal axis is particle size. The continuous gradation curve is to be discretized into n size-classes of particles; particles of each class are considered to be equal size. The solid fraction y_i for each size-class of particles with particle size d_i can be determined by the following process.

Note that the particle size is sorted by $d_1 > d_2 > \ldots > d_n$ for a soil mixture. Divided the gradation curve into n divisions, there are n+1 ticks: $\hat{d}_1$, … $\hat{d}_n$, $\hat{d}_{n+1}$ (subscript order is from large size to small size). The i-th division has a size range from $\hat{d}_{i+1}$ to $\hat{d}_i$. Using a geometric series for the values of the tick marks, so that for all divisions, the ratios of $\hat{d}_i / \hat{d}_{i+1}$ are constant. This ratio can be determined from the total range $\hat{d}_1$, $\hat{d}_{n+1}$and the number of divisions n, given by

$$\frac{\hat{d}_i}{\hat{d}_{i+1}} = \left(\frac{\hat{d}_1}{\hat{d}_{n+1}}\right)^{1/n} \quad (i = 1, 2, \ldots, n+1) \tag{B.1}$$

Thus, the i-th tick mark $\hat{d}_i$ is related to $\hat{d}_1$, $\hat{d}_{n+1}$ and n by

$$\hat{d}_i = \hat{d}_1 \left(\frac{\hat{d}_{n+1}}{\hat{d}_1}\right)^{(i-1)/n} \quad (i = 1, 2, \ldots, n+1) \tag{B.2}$$

The particle size d_i for the i-th division is the geometric average of its particle size range.

$$d_i = \sqrt{\hat{d}_i \hat{d}_{i+1}} \tag{B.3}$$

In order to minimize the errors induced by discretization, the number of division n should be large enough to assure that $d_i/d_{i\text{-}1} < 1.1$ suggested by Chang et al. (2017). The soil can thus be considered as a mixture consisting of n-component particles with particle size d_i (i = 1 to n). Each component is represented by a division of the gradation curve. The solid volume fraction y_i for each component in the mixture can be calculated from the gradation curve as shown in Fig. B.1:

$$y_i = F_i - F_{i+1} \tag{B.4}$$

where F_i is the value on the vertical axis of the gradation curve (in percentage) corresponding to size $\hat{d}_i$ on the horizontal axis.

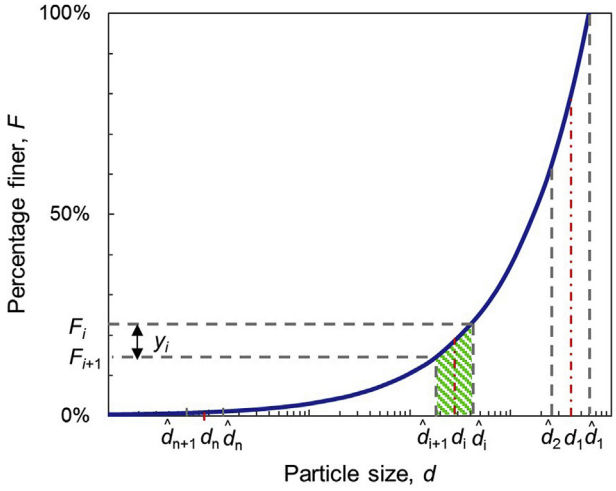

Fig. B.1. Discretization for a gradation curve.

Appendix C. Other CSL formulations

In the following, using the logarithmic formula in Eq. (A.9) and the sigmoid formula in Eq. (A.11) respectively, the CSLs for various GSDs were predicted by the proposed model for Quartz silty sand (Papadopoulou and Tika, 2008), Camargue silty sand (Nguyen et al., 2017), DEM (Li et al., 2015) and glass beads (Li et al., 2015). The parameters for CSL of mono-sized packing and the parameters s and t are listed in Table C.1. Note that the parameters s and t in the model for each material are same as that used in Table 2.

The predicted CSLs for each material in the form of logarithmic formula in Eq. (A.9) are plotted in Fig. C.1. The CSLs for each material become a series of straight lines in the $e - \log p'$ plane. Fig. C.1 shows that there is a good agreement between predicted and experimental results.

The predicted CSLs for each material in the form of sigmoid formula in Eq. (A.11) are plotted in Fig. C.2. The CSLs for quartz silty sand and Camargue silty sand are a series of curved lines in the $e-\log p'$ plane. Fig. C.2 shows that there is a good agreement between predicted and experimental results. Note that, in contrast to these two silty sands, the CSLs for glass beads and DEM are flat in the $e-\log p'$ plane, which is captured by the low values of ξ for glass beads and DEM. Thus, the sigmoid formula provides a better fit for curved CSLs.

Table C.1
Input parameters for each material.

Soil type	Ref.	Eq. (A.9)		Eq. (A.11)				s	t
		$\bar{e}_{ref}$	$\bar{\lambda}$	$\bar{e}_{cu}$	$\bar{e}_{cmax}$	$\bar{m}$	$\bar{\xi}$		
Glass beads	Li et al. (2015)	0.772	0.019	0.40	1.05	13	0.085	2.3	2.2
DEM	Li et al. (2015)	0.823	0.008	0.60	1.04	16	0.042	1.8	1.8
Quartz silty sand	Papadopoulou and Tika (2008)	0.981	0.047	0.45	0.85	35	0.380	5.0	4.0
Camargue silty sand	Nguyen et al. (2017)	1.025	0.025	0.48	1.00	83	0.425	7.0	3.5

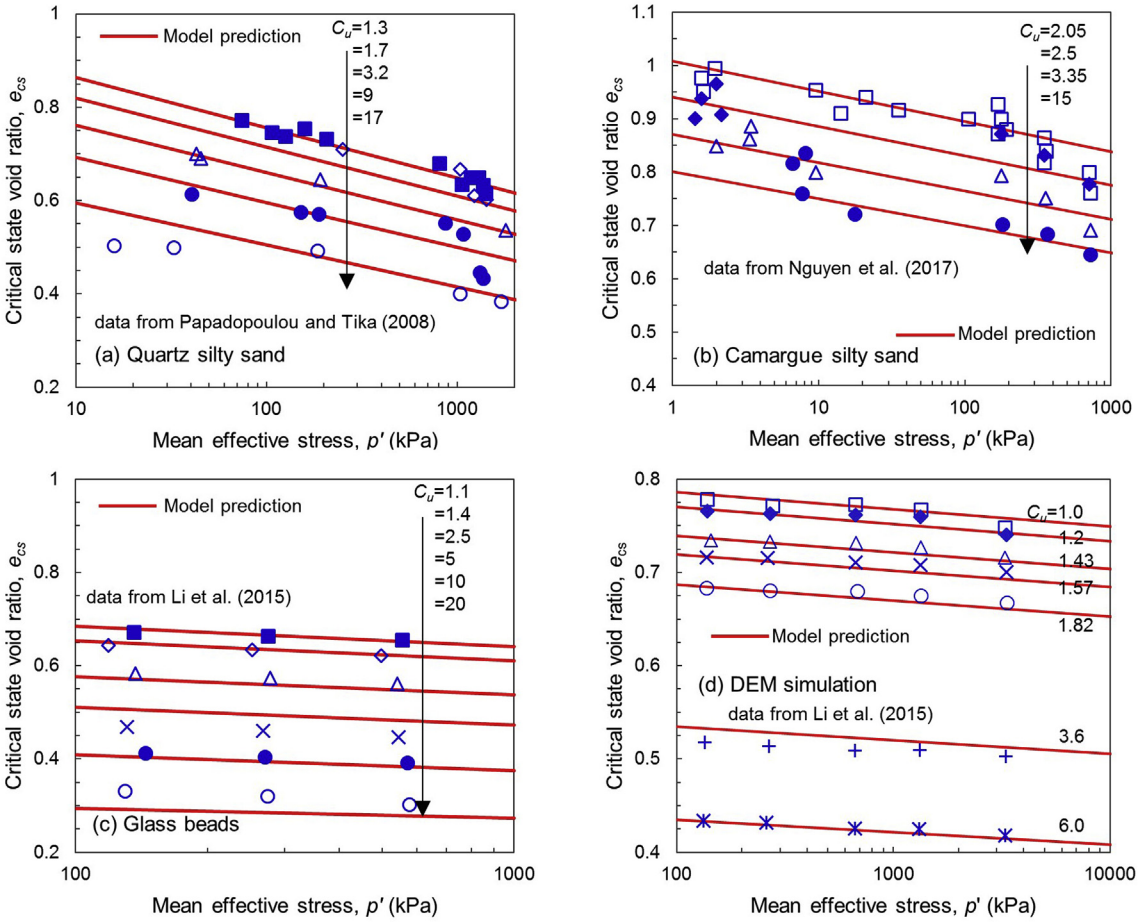

Fig. C.1. Comparison of predicted and measured CSLs using the logarithmic formula in Eq. (A.9).

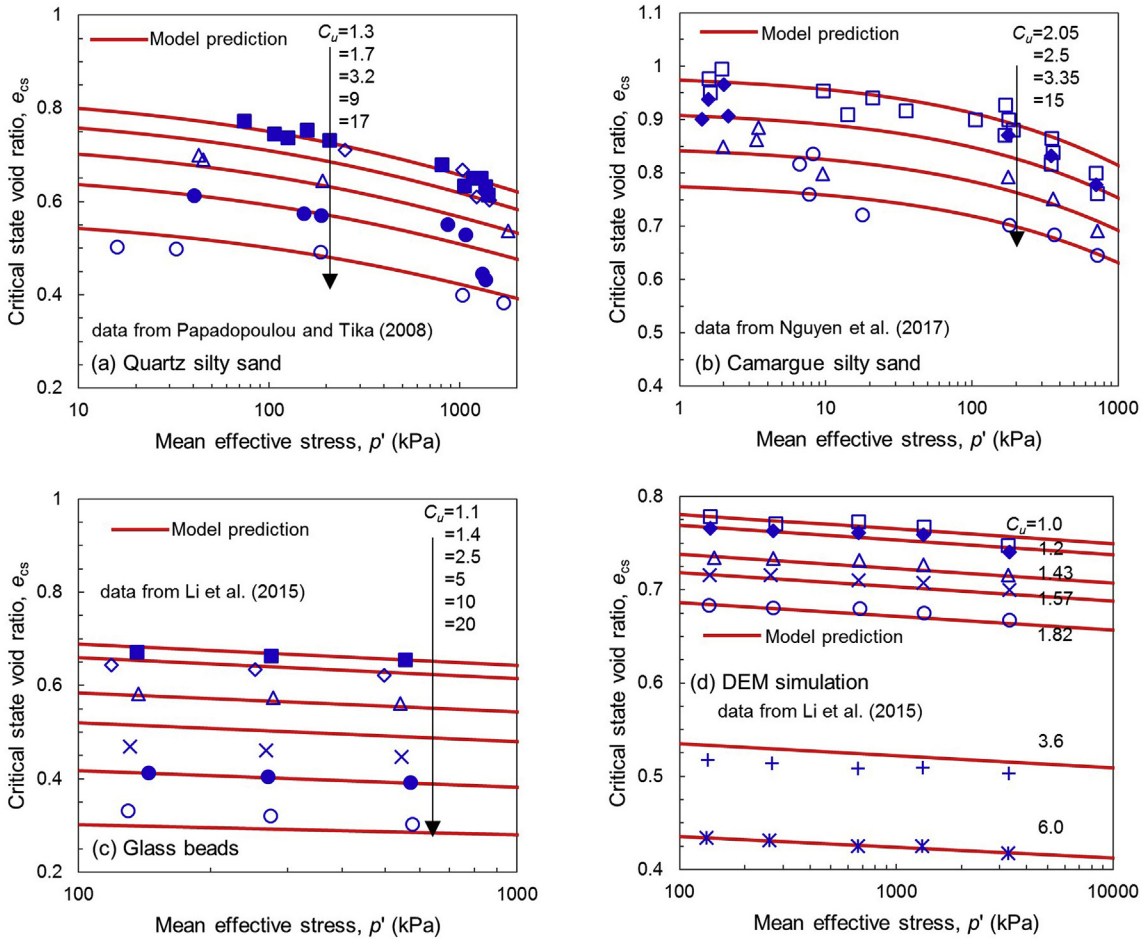

Fig. C.2. Comparison of predicted and measured CSLs using the sigmoid formula in Eq. (A.11).

References

ASTM D 2487-06, 2006. Standard Practice for Classification of Soils for Engineering Purposes (Unified Soil Classification System). ASTM International, West Conshohocken, PA, USA.

Bandini, V., Coop, M.R., 2011. The influence of particle breakage on the location of the critical state line of sands. Soils Found. 51, 591–600. https://doi.org/10.3208/sandf.51.591.

Been, K., Jefferies, M.G., 1985. A state parameter for sands. Geotechnique 35, 99–112.

Been, K., Jefferies, M.G., Hachey, J., 1991. The critical state of sands. Geotechnique 41, 365–381. https://doi.org/10.1680/geot.1991.41.3.365.

Biarez, J., Hicher, P.-Y., 1994. Elementary Mechanics of Soil Behaviour: Saturated Remoulded Soils. Balkema, Rotterdam.

Carraro, J.A.H., Asce, A.M., Prezzi, M., Asce, A.M., Salgado, R., Asce, M., 2009. Shear strength and stiffness of sands containing plastic or nonplastic fines. J. Geotech. Geoenviron. Eng. 135, 1167–1178.

Chang, C.S., Deng, Y., Yang, Z., 2017. Modeling of minimum void ratio for granular soil with effect of particle size distribution. J. Eng. Mech. 143, 04017060. https://doi.org/10.1061/(ASCE)EM.1943-7889.0001270.

Chang, C.S., Meidani, M., 2013. Dominant grains network and behavior of sand-silt mixtures: stress-strain modeling. Int. J. Numer. Anal. Methods Geomech. 37, 2563–2589. https://doi.org/10.1002/nag.2152.

Chang, C.S., Wang, J.-Y., Ge, L., 2015. Modeling of minimum void ratio for sand–silt mixtures. Eng. Geol. 196, 293–304. https://doi.org/10.1016/j.enggeo.2015.07.015.

Chang, C.S., Wang, J.-Y., Ge, L., 2016. Maximum and minimum void ratios for sand-silt mixtures. Eng. Geol. 211, 7–18. https://doi.org/10.1016/j.enggeo.2016.06.022.

Ciantia, M.O., Arroyo, M., O'Sullivan, C., Gens, A., Liu, T., 2019. Grading evolution and critical state in a discrete numerical model of Fontainebleau sand. Geotechnique 69, 1–15. https://doi.org/10.1680/jgeot.17.P.023.

Cubrinovski, M., Ishihara, K., 2002. Maximum and minimum void ratio characteristics of sands. Soils Found. 42, 65–78. https://doi.org/10.3208/sandf.42.6_65.

Daouadji, A., Hicher, P.Y., Rahma, A., 2001. An elastoplastic model for granular materials taking into account grain breakage. Eur. J. Mech. 20, 113–137.

Einav, I., 2007. Breakage mechanics—Part I: theory. J. Mech. Phys. Solids 55, 1274–1297. https://doi.org/10.1016/j.jmps.2006.11.003.

Gudehus, G., 1997. Attractors, percolation thresholds and phase limits of granular soils. In: Behringer, R.P., Jenkins, J.T. (Eds.), Powders & Grains 97. Rotterdam, Balkema, pp. 169–183.

Hardin, B.O., 1985. Crushing of soil particles. J. Geotech. Eng. 111, 1177–1192. https://doi.org/10.1061/(ASCE)0733-9410(1985)111:10(1177).

Hu, W., Yin, Z., Dano, C., Hicher, P.Y., 2011. A constitutive model for granular materials considering grain breakage. Sci. China Technol. Sci. 54, 2188–2196. https://doi.org/10.1007/s11431-011-4491-0.

Hyodo, M., Nakata, Y., Yoshimoto, N., Kato, Y., Okabayashi, T., 2001. The role of fines in the shear and liquefaction of a volcanic soil 'Shirasu' as a reclamation material. In: Proc. 11th Int. Offshore and Polar Engineering Conf. Norway, pp. 501–507.

Imam, S.R., Morgenstern, N.R., Robertson, P.K., Chan, D.H., 2005. A critical-state constitutive model for liquefiable sand. Can. Geotech. J. 42, 830–855. https://doi.org/10.1139/t05-014.

Jefferies, M., Been, K., 2006. Soil Liquefaction: A Critical State Approach. Taylor & Francis, New York.

Konrad, J.-M., 1998. Sand state from cone penetrometer tests: a framework considering grain crushing stress. Geotechnique 48, 201–215. https://doi.org/10.1680/geot.1998.48.2.201.

Lade, P.V., Liggio, C.D., Yamamuro, J.A., 1998. Effects of non-plastic fines on minimum and maximum void ratios of sand. Geotech. Test J. 21, 336–347. https://doi.org/10.1520/GTJ11373J.

Lade, P.V., Yamamuro, J.A., Bopp, P.A., 1996. Significance of particle crushing in granular materials. J. Geotech. Geoenviron. Eng. 122, 309–316. https://doi.org/10.1061/(ASCE)0733-9410(1996)122:4(309).

Li, G., 2013. Étude de l'influence de l'étalement granulometrique sur le comportement mecanique des materiaux granulaires. Ecole Central de Nantes, Nantes, France.

Li, G., Liu, Y., Dano, C., Hicher, P., 2015. Grading-dependent behavior of granular Materials : from discrete to continuous modeling. J. Eng. Mech. 141, 1–15. https://doi.org/10.1061/(ASCE)EM.1943-7889.0000866.

Li, X.S., Wang, Y., 1998. Linear representation of steady-state line for sand. J. Geotech. Geoenviron. Eng. 124, 1215–1217. https://doi.org/10.1061/(ASCE)1090-0241(1998)124:12(1215).

Marsal, R.J., 1963. Large scale testing of rockfill materials. J. Soil Mech. Found. 93, 27–43.
Muir Wood, D., Maeda, K., 2008. Changing grading of soil: effect on critical states. Acta Geotech 3, 3–14. https://doi.org/10.1007/s11440-007-0041-0.
Nguyen, T., Benahmed, N., Hicher, P., 2017. Determination of the equivalent intergranular void ratio - application to the instability and the critical state of silty sand. In: Radjai, F., et al. (Eds.), Powders and Grains 2017 – 8th International Conference on Micromechanics on Granular Media. EDP Sciences, Montpellier, France, p. 02019. https://doi.org/10.1051/epjconf/201714002019.
Papadopoulou, A., Tika, T., 2008. The effect of fines on critical state and liquefaction resistance characteristics of non-plastic silty sands. Soils Found. 48, 713–725. https://doi.org/10.3208/sandf.47.887.
Riemer, M.F., Seed, R.B., 1997. Factors affecting apparent position of steady-state line. J. Geotech. Geoenviron. Eng. 123, 281–288.
Roscoe, K.H., Schofield, A.N., Wroth, C.P., 1958. On the yielding of soils. Geotechnique 1, 22–53.
Russell, A.R., Khalili, N., 2004. A bounding surface plasticity model for sands exhibiting particle crushing. Can. Geotech. J. 41, 1179–1192. https://doi.org/10.1139/t04-065.
Sadrekarimi, A., Olson, S.M., 2011. Yield strength ratios, critical strength ratios, and brittleness of sandy soils from laboratory tests. Can. Geotech. J. 48, 493–510. https://doi.org/10.1139/T10-078.
Sammis, C., King, G., Biegel, R., 1987. The kinematics of gouge deformation. Pure Appl. Geophys. 125, 777–812. https://doi.org/10.1007/BF00878033.
Schofield, A.N., Wroth, C.P., 1968. Critical State Soil Mechanics. McGraw-Hill, Maidenhead, England.
Tengattini, A., Das, A., Einav, I., 2016. A constitutive modelling framework predicting critical state in sand undergoing crushing and dilation. Geotechnique 66, 695–710. https://doi.org/10.1680/jgeot.14.P.164.
Thevanayagam, S., Shenthan, T., Mohan, S., Liang, J., 2002. Undrained fragility of clean sands, silty sands, and sandy silts. J. Geotech. Geoenviron. Eng. 128, 849–859. https://doi.org/10.1061/(ASCE)1090-0241(2002)128:10(849.
Torres-Cruz, L.A., Geyer, S., Mackechnie, P.R., 2017. Effect of the minimum void ratio on the vertical intercept of the steady state line of non-plastic soils. J. South African Inst. Civ. Eng. 59, 59–64. https://doi.org/10.17159/2309-8775/2017/v59n2a7.
Verdugo, R., Ishihara, K., 1996. The steady state of sandy soils. Soils Found. 36, 81–91. https://doi.org/10.1248/cpb.37.3229.
Xiao, Y., Liu, H., 2017. Elastoplastic constitutive model for rockfill materials considering particle breakage. Int. J. Geomech. 17, 04016041. https://doi.org/10.1061/(ASCE)GM.1943-5622.0000681.
Xiao, Y., Liu, H., Desai, C.S., Sun, Y., Liu, H., 2016a. Effect of intermediate principal-stress ratio on particle breakage of rockfill material. J. Geotech. Geoenviron. Eng. 142, 06015017. https://doi.org/10.1061/(ASCE)GT.1943-5606.0001433.
Xiao, Y., Liu, H., Ding, X., Chen, Y., Jiang, J., Zhang, Wengang, 2016b. Influence of particle breakage on critical state line of rockfill. Material. Int. J. Geomech. 16, 04015031. https://doi.org/10.1061/(ASCE)GM.1943-5622.0000538.
Xiao, Y., Sun, Y., Hanif, K.F., 2015. A particle-breakage critical state model for rockfill material. Sci. China Technol. Sci. 58, 1125–1136. https://doi.org/10.1007/s11431-015-5831-2.
Yilmaz, Y., 2009. A study on the limit void ratio characteristics of medium to fine mixed graded sands. Eng. Geol. 104, 290–294. https://doi.org/10.1016/j.enggeo.2008.11.009.
Youd, T.L., 1973. Factors controlling maximum and minimum densities of sands. In: Evaluation of Relative Density and its Role in Geotechnical Projects Involving Cohesionless Soils, STP, vol. 523. ASTM International, West Conshohocken, PA, pp. 98–112. https://doi.org/10.1520/STP37866S.
Yu, F.W., 2017. Particle breakage and the critical state of sands. Geotechnique 67, 713–719. https://doi.org/10.1016/j.sandf.2014.04.016.
Yu, F.-W., Su, L.-J., 2016. Particle breakage and the mobilized drained shear strengths of sand. J. Mt. Sci. 13, 1481–1488. https://doi.org/10.1007/s11629-016-3870-1.
Zhou, W., Liu, J., Ma, G., Chang, X., 2017. Three-dimensional DEM investigation of critical state and dilatancy behaviors of granular materials. Acta Geotech 12, 527–540. https://doi.org/10.1007/s11440-017-0530-8.